EXPERIMENTAL AND NUMERICAL LOCALIZATION OF NOISE SOURCES FOR CYLINDER IN ROUND JET

V. Kopiev[1], G. Faranosov[1], N. Ostrikov[1], M. Zaitsev[1]
I. Abalakin[2], A. Gorobets[2], T. Kozubskaya[2]
[1]TSAGI, Moscow Branch, [2]IPM RAS

Experiment
- new measurements of dipole noise (model dipole and broadband dipole);
- displacement of the dipole source in jet/rod interaction problem far downstream;

Theory
- physical background of the problem;
- explanation of experimental results as self-tuning effect for reflected dipoles;
  - dipole source displacement;
  - noise reduction for truncated geometry;
- role of the refraction for the dipole in jet;

Numerical simulations
- CAA: ILES of the flow past regular cylinders;
- Direct computation of multipole source density;

Identification of dipole displacement

Experiment

Sound field produced by arbitrary harmonic source

$$P_\omega = e^{-i\omega t} \sum_{l=0}^{\infty} \sum_{m=-l}^{l} \frac{c_{lm}}{\sqrt{r}} H_{l+1/2}^{(1)}(kr) Y_l^m(\varphi, \chi)$$

$$Y_l^m = P_l^{|m|}(\cos \chi) e^{im\varphi}$$

In the far field:

$$P_\omega = \frac{e^{ikr-i\omega t}}{r} \{ a_{00} + \left[a_{10} P_1^0 + (a_{11} \cos \varphi + b_{11} \sin \varphi) P_1^1 \right] +$$

$$+ \left[a_{20} P_2^0 + (a_{21} \cos \varphi + b_{21} \sin \varphi) P_2^1 + (a_{22} \cos 2\varphi + b_{22} \sin 2\varphi) P_2^2 \right] + ... \}$$

or

$$P_\omega = \frac{e^{ikr-i\omega t}}{r} \{ \left[a_{00} + a_{10} P_1^0 + a_{20} P_2^0 + ... \right] +$$

$$\cos \varphi \left[a_{11} P_1^1 + a_{21} P_2^1 + ... \right] + \sin \varphi \left[b_{11} P_1^1 + b_{21} P_2^1 + ... \right] +$$

$$\cos 2\varphi \left[a_{22} P_2^2 + a_{31} P_3^2 + ... \right] + \sin 2\varphi \left[b_{22} P_2^2 + b_{32} P_3^2 + ... \right]$$

$$+ \cos 3\varphi \left[a_{33} P_3^3 + ... \right] + ... \} = \frac{e^{ikr-i\omega t}}{r} \{ A_0(\chi) + A_1(\chi) \cos \varphi + B_1(\chi) \sin \varphi + ... \}$$

Fourier-transformation of arbitrary sound field

$$P(\varphi,\chi,t) = A_0 + A_1 \cos\varphi + B_1 \sin\varphi + A_2 \cos 2\varphi + B_2 \sin 2\varphi + \ldots$$

$$P(\varphi_i, \chi, t) = s_i(t)$$

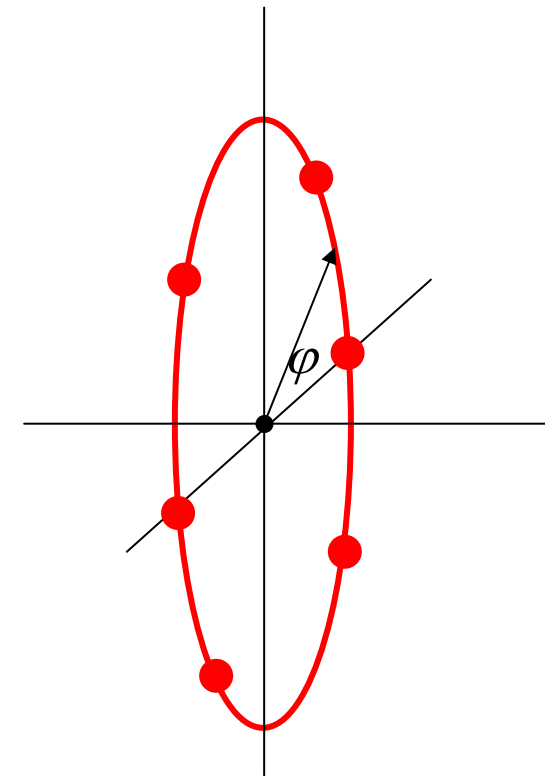$$a_0(t) = \frac{1}{\sqrt{6}} \sum_{i=1}^{6} s_i = A_0 + O(A_6, A_{12}, \ldots)$$

$$a_1(t) = \frac{1}{\sqrt{3}}\left(s_1 + \frac{1}{2}s_2 - \frac{1}{2}s_3 - s_4 - \frac{1}{2}s_5 + \frac{1}{2}s_6 \right) = A_1 + O(A_5, A_{13}, \ldots)$$

$$b_1(t) = \left(\frac{1}{2}s_2 + \frac{1}{2}s_3 - \frac{1}{2}s_5 - \frac{1}{2}s_6 \right) = B_1 + O(B_5, B_{13}, \ldots)$$

$$a_2(t) = \frac{1}{\sqrt{3}}\left(s_1 - \frac{1}{2}s_2 - \frac{1}{2}s_3 + s_4 - \frac{1}{2}s_5 - \frac{1}{2}s_6 \right) = A_2 + O(A_4, A_{10}, \ldots)$$
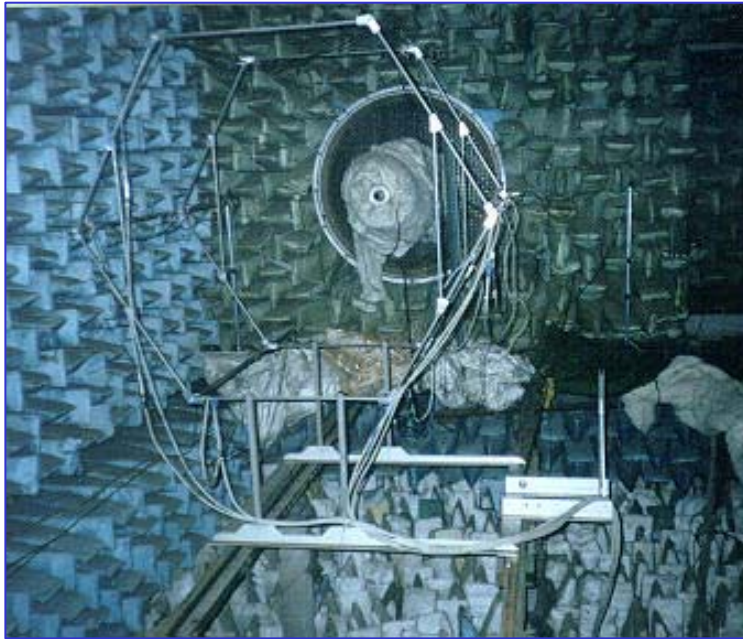
$$b_2(t) = \left(\frac{1}{2}s_2 - \frac{1}{2}s_3 + \frac{1}{2}s_5 - \frac{1}{2}s_6 \right) = B_2 + O(B_4, B_{10}, \ldots)$$

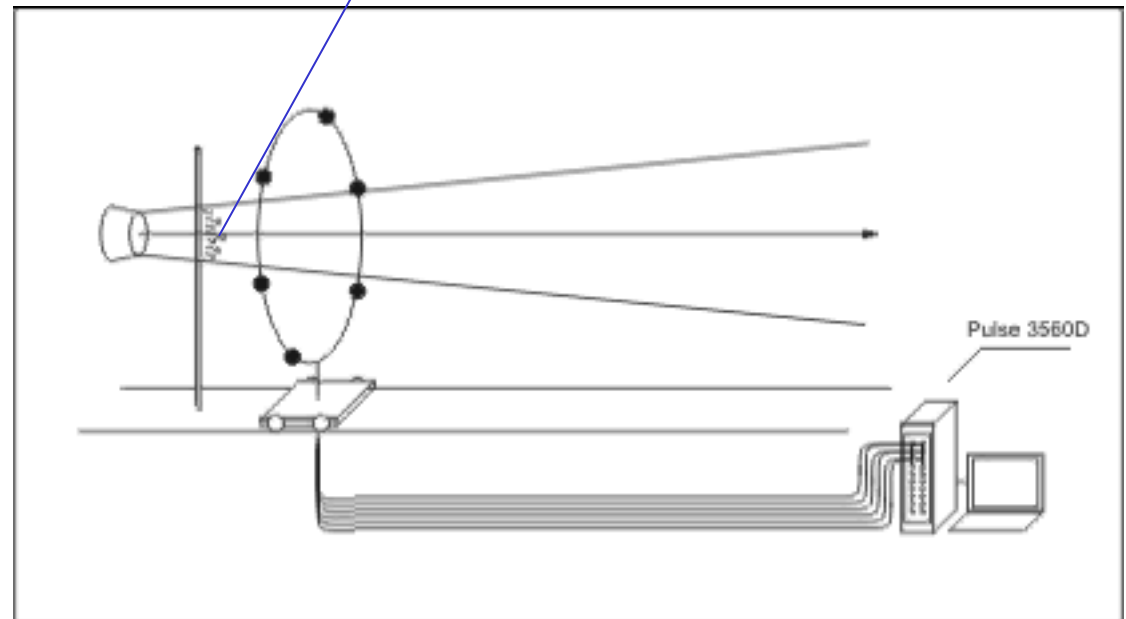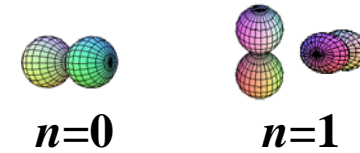$$a_3(t) = \frac{1}{\sqrt{6}}(s_1 - s_2 + s_3 - s_4 + s_5 - s_6) = A_3 + O(A_9, A_{15}, \ldots)$$

easy to check that $\quad s^2 = a_0^2 + a_1^2 + b_1^2 + a_2^2 + b_2^2 + a_3^2 \equiv \sum_{1}^{6} s_i^2$

Microphone array in TsAGI anechoic chamber

$n=0$ $n=1$

The microphone array is shifted along the axis z, sweeping over the cylindrical surface in the far field covering up to 50 calibers along the axis.
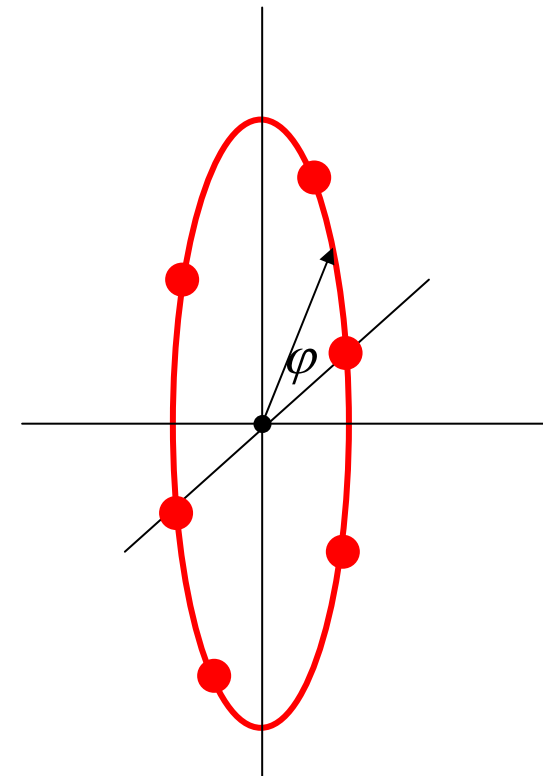
Pulse 3560D

Fourier-transformation of arbitrary sound field

$$P(\varphi,\chi,t) = A_0 + A_1 \cos\varphi + B_1 \sin\varphi + A_2 \cos 2\varphi + B_2 \sin 2\varphi + ...$$

$$P(\varphi_i,\chi,t) = s_i(t)$$

$$a_0(t) = \frac{1}{\sqrt{6}} \sum_{i=1}^{6} s_i = A_0 + O(A_6, A_{12}, ...)$$

$$a_1(t) = \frac{1}{\sqrt{3}}\left(s_1 + \frac{1}{2}s_2 - \frac{1}{2}s_3 - s_4 - \frac{1}{2}s_5 + \frac{1}{2}s_6 \right) = A_1 + O(A_5, A_{13}, ...)$$

$$b_1(t) = \left(\frac{1}{2}s_2 + \frac{1}{2}s_3 - \frac{1}{2}s_5 - \frac{1}{2}s_6 \right) = B_1 + O(B_5, B_{13}, ...)$$

$$a_2(t) = \frac{1}{\sqrt{3}}\left(s_1 - \frac{1}{2}s_2 - \frac{1}{2}s_3 + s_4 - \frac{1}{2}s_5 - \frac{1}{2}s_6 \right) = A_2 + O(A_4, A_{10}, ...)$$

$$b_2(t) = \left(\frac{1}{2}s_2 - \frac{1}{2}s_3 + \frac{1}{2}s_5 - \frac{1}{2}s_6 \right) = B_2 + O(B_4, B_{10}, ...)$$

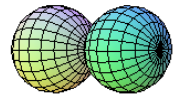$$a_3(t) = \frac{1}{\sqrt{6}}(s_1 - s_2 + s_3 - s_4 + s_5 - s_6) = A_3 + O(A_9, A_{15}, ...)$$

easy to check that $\quad s^2 = a_0^2 + a_1^2 + b_1^2 + a_2^2 + b_2^2 + a_3^2 \equiv \sum_1^6 s_i^2$
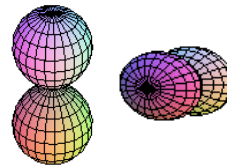
Dipole directivities

$$P_\omega = \frac{e^{ikr - i\omega t}}{r} \left[a_{10} P_1^0 (\cos \chi) + (a_{11} \cos \varphi + b_{11} \sin \varphi) P_1^1 (\cos \chi) \right]$$

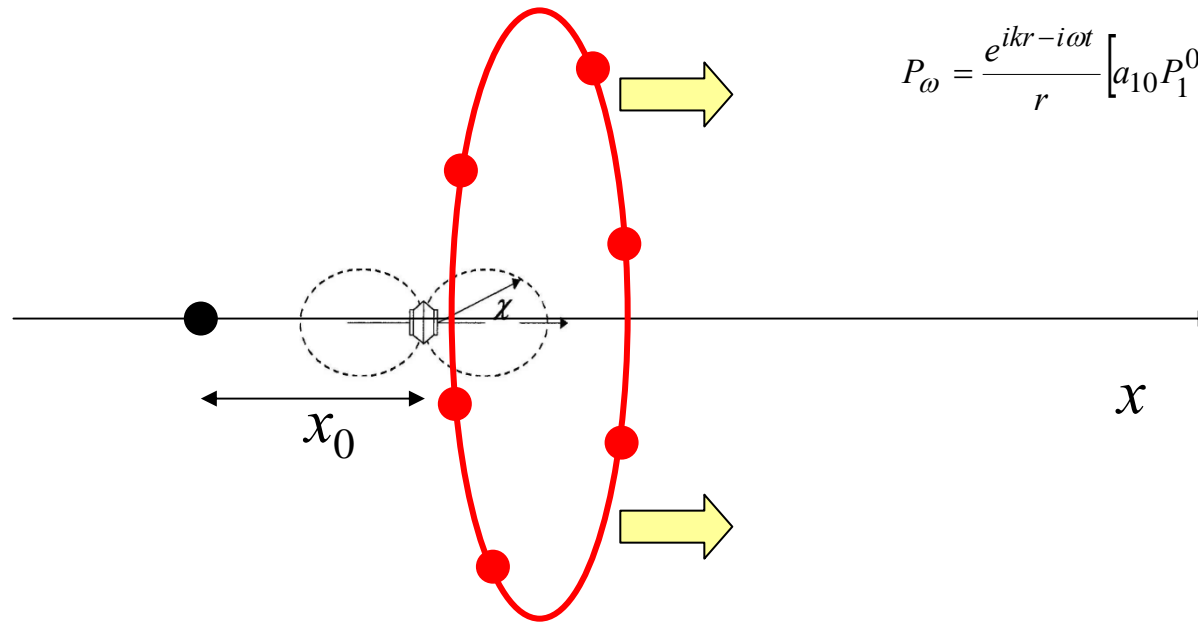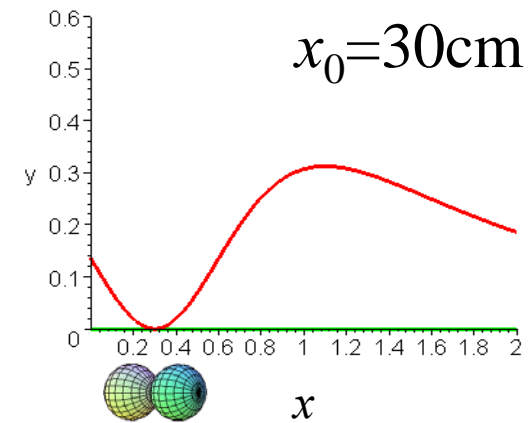where $P_1^0 = \cos \chi, \quad P_1^1 = \sin \chi$
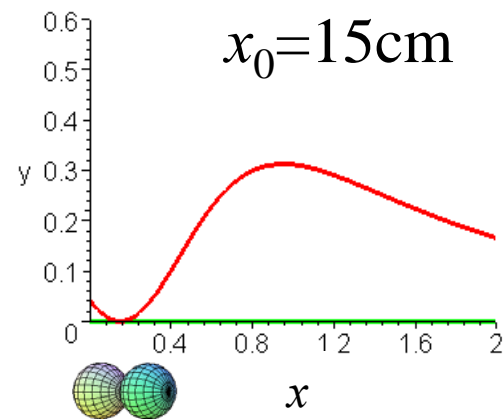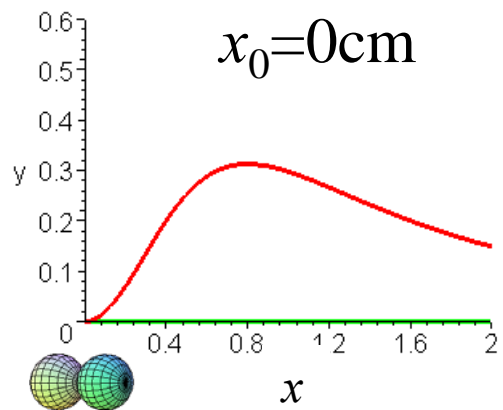

$n=0$

$n=1$

Model dipole source

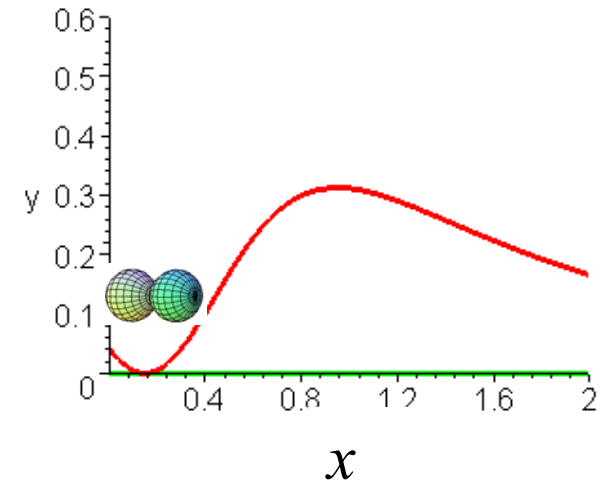(two loudspeakers in opposite phases)

Microphone array and dipole source

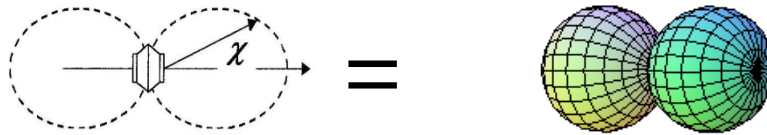$$P_\omega = \frac{e^{ikr-i\omega t}}{r}\left[a_{10}P_1^0(\cos\chi) + (a_{11}\cos\varphi + b_{11}\sin\varphi)P_1^1(\cos\chi)\right]$$
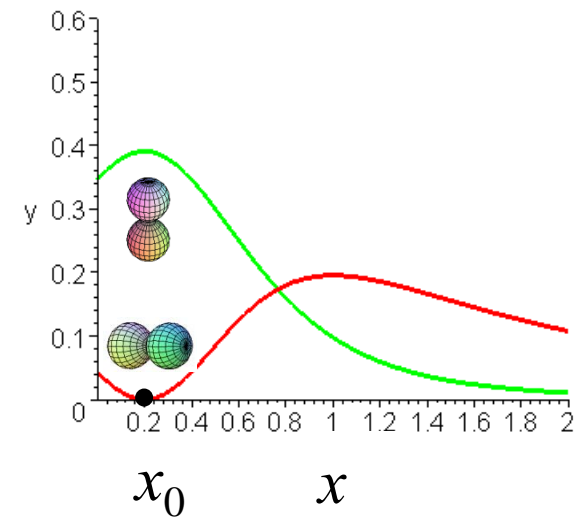
x_0

x

$x_0=0$cm

$x_0=15$cm

$x_0=30$cm

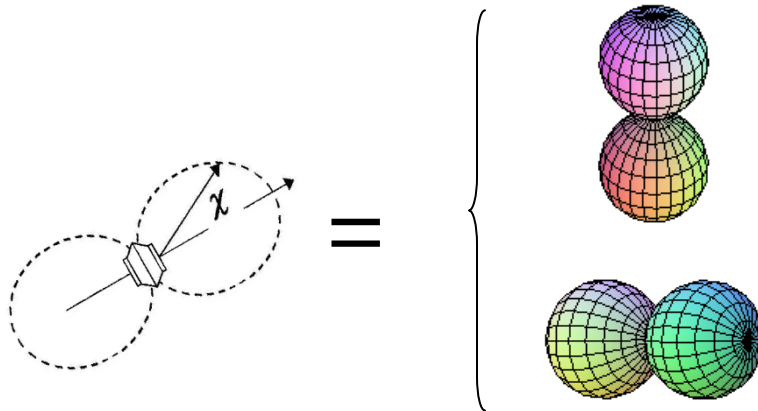# Experimental diagnostics of dipole radiation

$$P_\omega = \frac{e^{ikr-i\omega t}}{r}\left[a_{10}P_1^0(\cos\chi)+(a_{11}\cos\varphi+b_{11}\sin\varphi)P_1^1(\cos\chi)\right]$$

$$P_\omega = \frac{e^{ikr-i\omega t}}{r}\left[a_{10}P_1^0(\cos\chi)+(a_{11}\cos\varphi+b_{11}\sin\varphi)P_1^1(\cos\chi)\right]$$

Comparison of theory and experiment for model dipole

Dipole oriented along x-axis (axisymmetrical case)
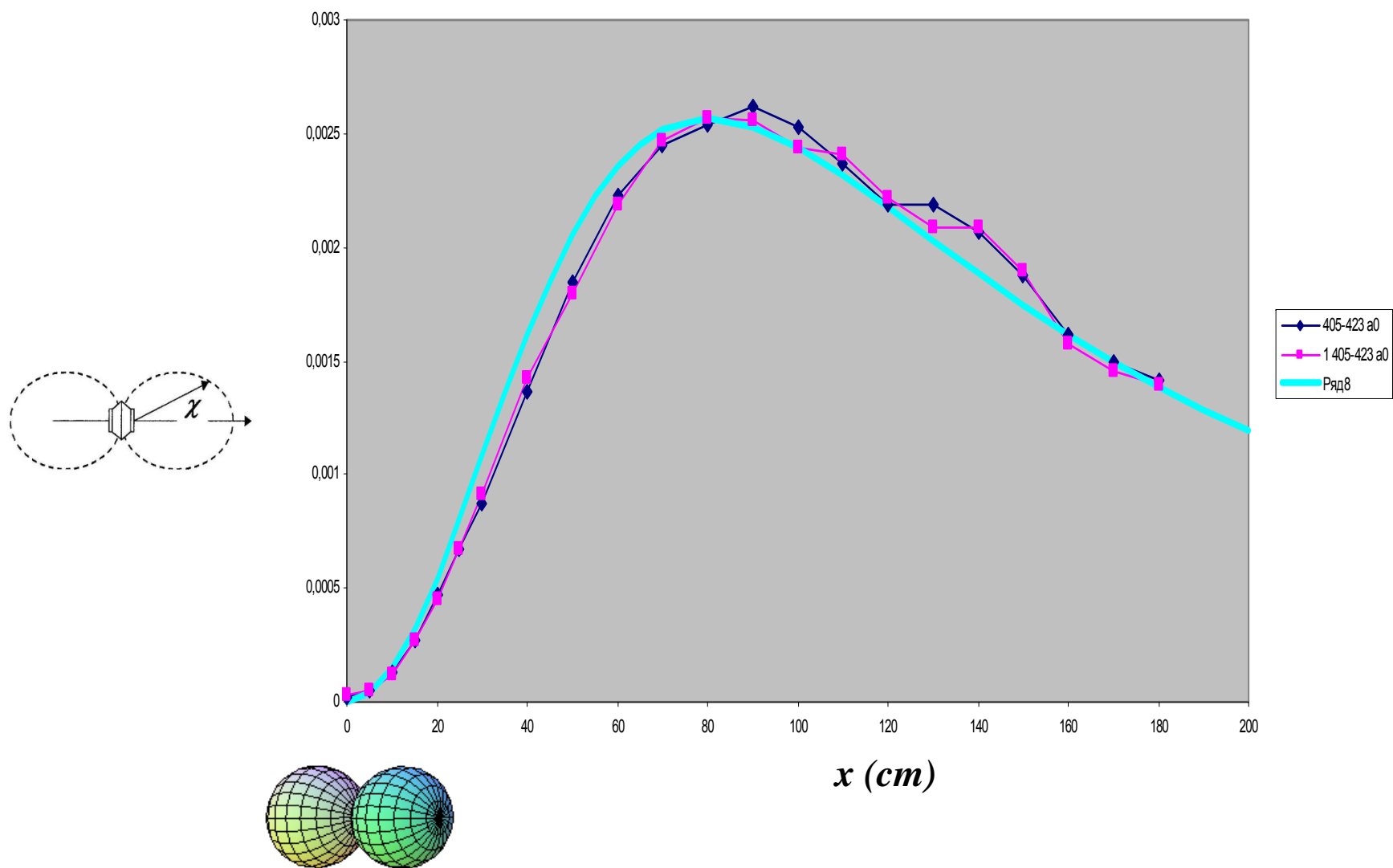
Comparison of theory and experiment for model dipole
Arbitrary oriented dipole (45° in *yz* plane)
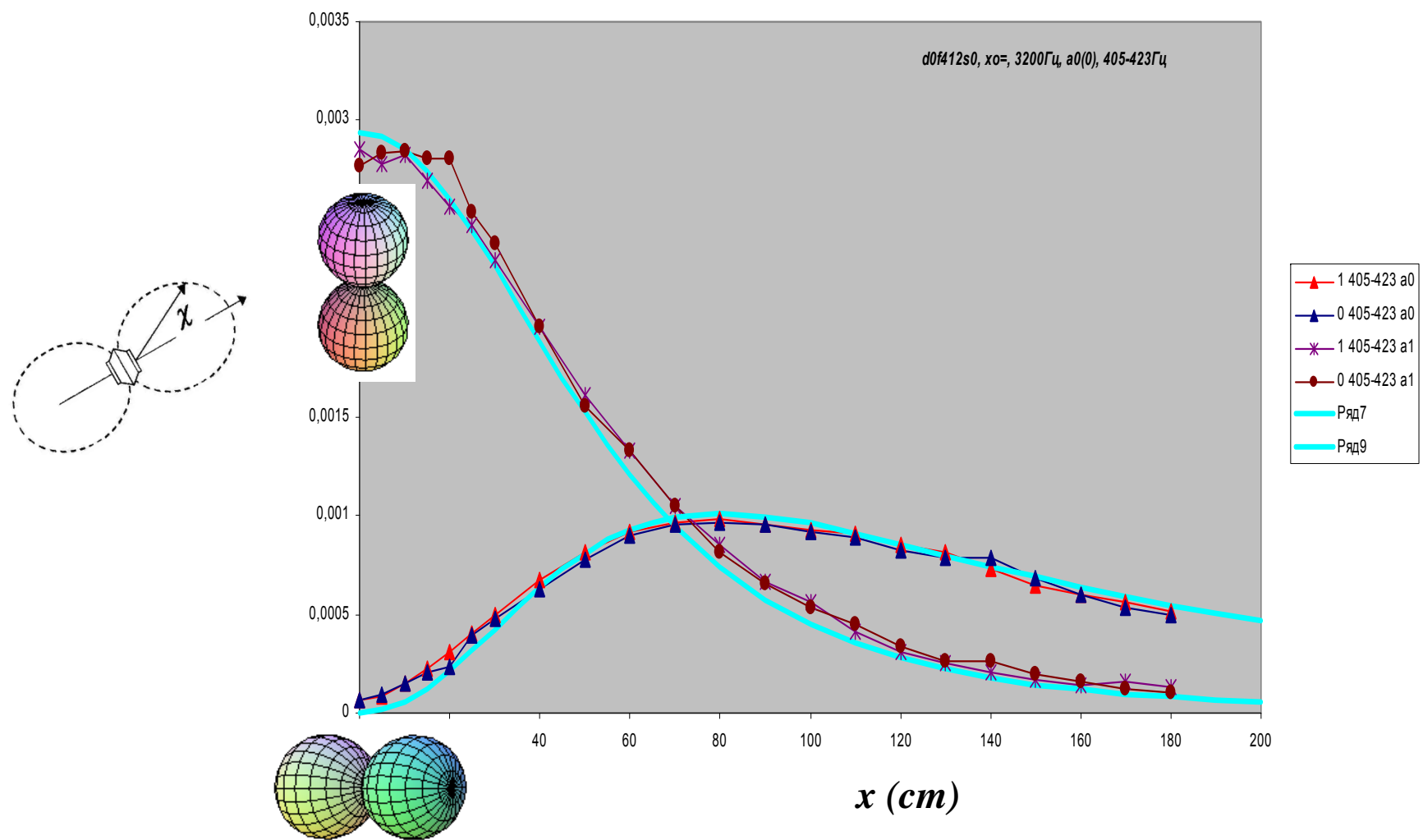
Dipole source produced by jet/rod interaction

(broadband dipole source)

Broadband dipole noise measurements (low frequencies).

Experimental setup,

D=4cm,

d_1=3mm

Broadband dipole noise measurements (low frequencies).

Experimental setup,

D=4cm,

d_1=3mm
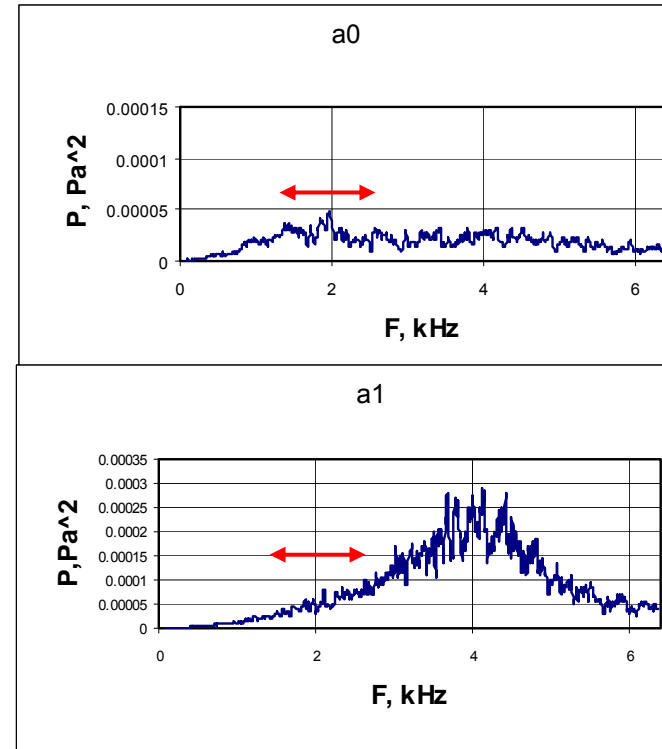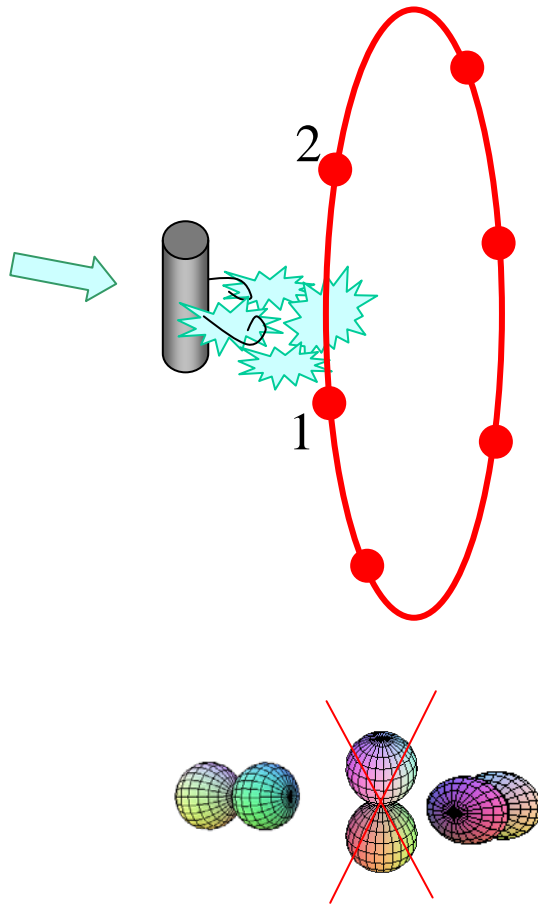
Displacement of the dipole source far downstream
Two modes (*n*=0) and (*n*=1) for rod diameter 3mm (with deleted the pure jet noise)
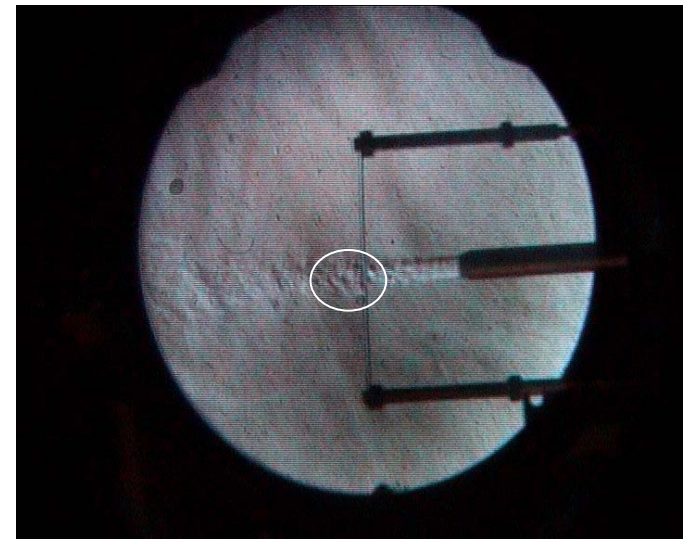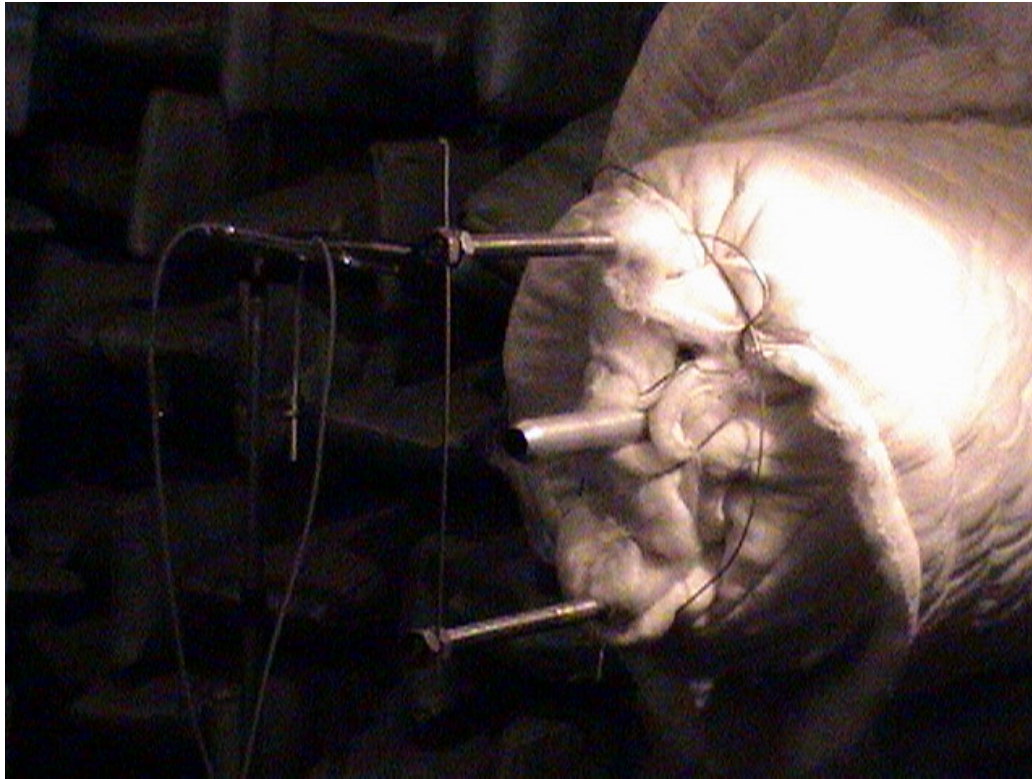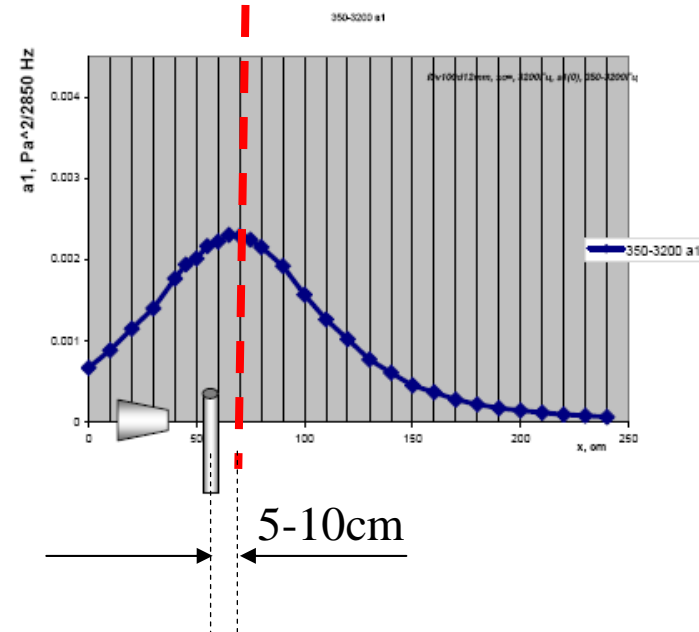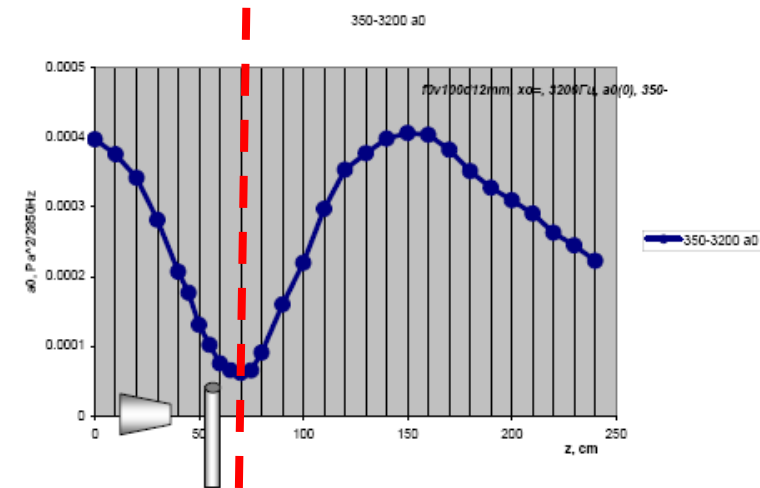

5-10cm

Analysis of multipole shift near the curved surface in long wave approximation

Curle's equation

$$4\pi \, p = \frac{x_j x_k}{c_0^2 \, x^2} \cdot \frac{1}{x} \frac{\partial^2}{\partial t^2} \int \left[T_{jk}\right] d^3 y + \frac{x_j}{c_0 x} \cdot \frac{1}{x} \frac{\partial}{\partial t} \int \left[p\right] \delta_{jk} d \, s_k = \frac{x_j x_k}{c_0^2 \, x} \frac{1}{x} \frac{\partial^2}{\partial t^2} \int \left[T_{jk}\right] d^3 y + \frac{x_j}{c_0 \, x} \cdot \frac{1}{x} \left[\frac{d \, F_j(t)}{d \, t}\right]$$

Analysis of multipole shift near the curved surface in long wave approximation

Curle's equation

$$4\pi\, p = \frac{x_j x_k}{c_0^2\, x^2} \cdot \frac{1}{x} \frac{\partial^2}{\partial t^2} \int \left[T_{jk}\right] d^3 y + \frac{x_j}{c_0 x} \cdot \frac{1}{x} \frac{\partial}{\partial t} \int [p]\delta_{jk} d\,s_k = \left(\frac{x_j x_k}{c_0^2\, x} \frac{1}{x} \frac{\partial^2}{\partial t^2} \int \left[T_{jk}\right] d^3 y + \frac{x_j}{c_0\, x} \cdot \frac{1}{x} \left[\frac{d\,F_j(t)}{d\,t}\right] \right)$$

$$M^2 \ll 1$$

Analysis of multipole shift near the curved surface in long wave approximation

Curle's equation

$$4\pi p = \frac{x_j x_k}{c_0^2 x^2} \cdot \frac{1}{x} \frac{\partial^2}{\partial t^2} \int [T_{jk}] d^3 y + \frac{x_j}{c_0 x} \cdot \frac{1}{x} \frac{\partial}{\partial t} \int [p] \delta_{jk} d s_k = \frac{x_j x_k}{c_0^2 x} \frac{1}{x} \frac{\partial^2}{\partial t^2} \int [T_{jk}] d^3 y + \frac{x_j}{c_0 x} \cdot \frac{1}{x} \left[\frac{d F_j(t)}{dt} \right]$$
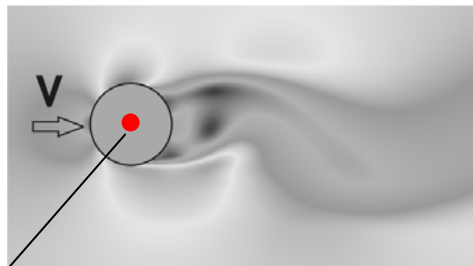
$$M^2 \ll 1$$

source location

?
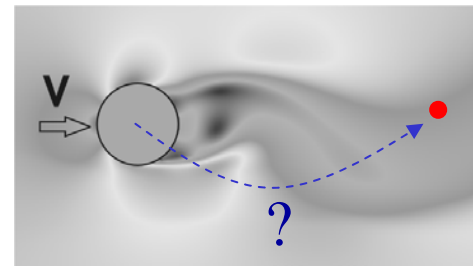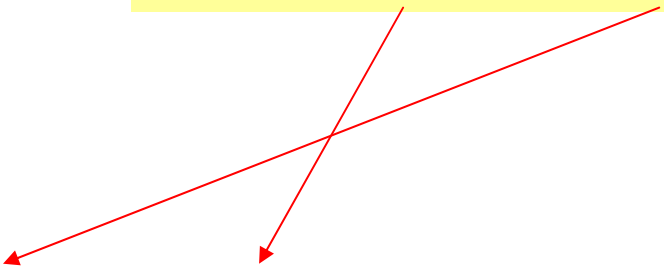
Theory

Why the dipole shifts?

Curle's equation

$$4\pi\, p = \frac{x_j x_k}{c_0^2\, x^2}\cdot\frac{1}{x}\frac{\partial^2}{\partial t^2}\int\left[T_{jk}\right]d^3 y + \frac{x_j}{c_0 x}\cdot\frac{1}{x}\frac{\partial}{\partial t}\int[p]\delta_{jk}d\, s_k = \frac{x_j x_k}{c_0^2\, x}\frac{1}{x}\frac{\partial^2}{\partial t^2}\int\left[T_{jk}\right]d^3 y + \frac{x_j}{c_0\, x}\cdot\frac{1}{x}\left[\frac{d\, F_j(t)}{d\, t}\right]$$

$$f(x_0) \approx f(0) + x_0 \cdot f'(0) + \ldots$$

dipole + quadrupole = shifted dipole

Incompressible sources: shift of the coordinate system
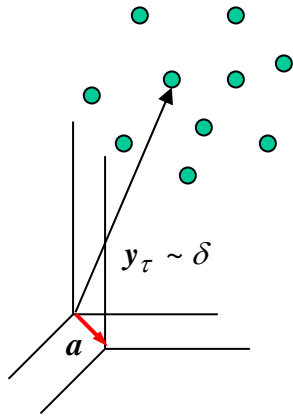
$$\varphi = \sum_{\tau} \frac{q_\tau}{|r - y_\tau|}$$

Expansion for $\quad r \gg \delta$

$$\varphi = \sum_{\tau} q_\tau \left(\frac{1}{r} + y_{\tau j} \frac{\partial(1/r)}{\partial x_j} + \frac{1}{2} y_{\tau j} y_{\tau k} \frac{\partial^2(1/r)}{\partial x_j \partial x_k} + ... \right) = \frac{1}{r} \left[Q - \frac{x_j D_j}{r^2} + \frac{x_j x_k}{r^2} P_{jk} + ... \right]$$

$y_\tau \sim \delta$

a

$$Q = \sum_{\tau} q_\tau$$

$$D_j = \sum_{\tau} q_\tau y_{\tau j}$$

$$P_{jk} = \sum_{\tau} q_\tau (y_{\tau j} y_{\tau k} - \frac{1}{3} y^2 \delta_{ij})$$

Transformation of multipole moments due to coordinate system shift

$$Q = 0, \quad P_{ij} = 0$$

was

$$\varphi = \frac{1}{r} \left[-\frac{x_i}{r^2} D_j \right]$$

$y_j = y_j + a_j$

$$\begin{cases} D'_j = \sum_{\tau} q_\tau (y_{\tau j} + a_j) = \sum_{\tau} q_\tau y_{\tau j} + Q a_j = D_j + Q a_j \\ P'_{jk} = P_{jk} + a_j D_k + a_k D_j + a_j a_k Q \end{cases}$$

become

$$\varphi = \frac{1}{r} \left[-\frac{x_i}{r^2} D_j + \frac{x_j x_k}{r^3} P_{jk} + ... \right]$$

$$D_j = D_j \qquad P_{jk} = a_k D_j$$

Multipoles near rigid cylinder
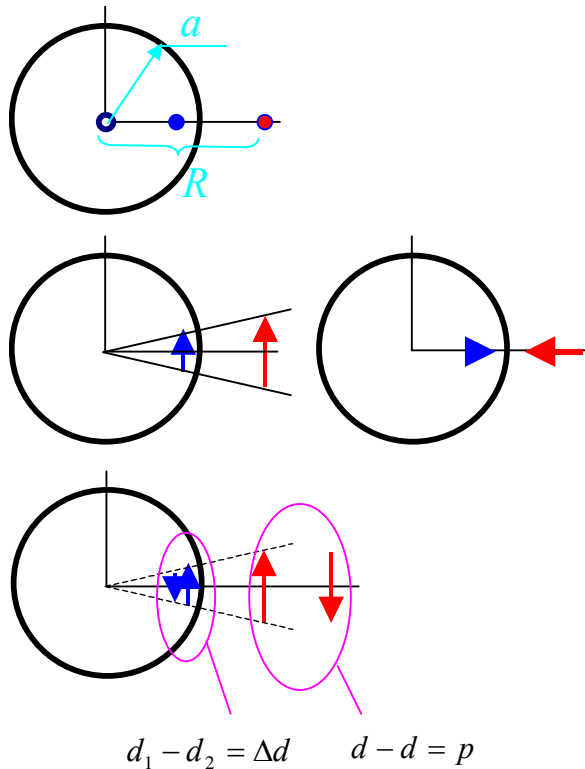
Dipole shifted by vector δ

$$\varphi_{y_j \to y_j + a_j} = \frac{1}{r}\left[-\frac{x_i}{r^2}D'_j + \frac{x_j x_k}{r^3}P'_{jk} + ...\right]$$

$$P_{jk} = \delta_k D_j$$

$$d_1 = ql(a/R)^2$$

$$d_2 = -ql(a/R)^2(1-2l/R)$$

$$\Delta d_y = \frac{2ql^2 a^2}{R^3} = \frac{2p a^2}{R^3}$$

$$-P_{xy} = P_{yx} = ql^2 = p$$

$d_1 - d_2 = \Delta d$ $d - d = p$
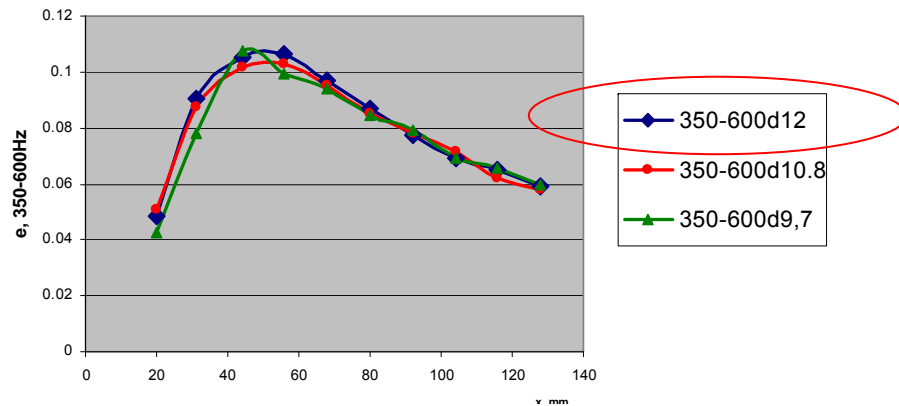
$$\delta = (a/2)(R/a)^3$$

$a\sim 1.5$mm, $R\sim 6$mm $\Rightarrow$ $\delta\sim 60$-80mm

e, 350-600Hz vs **x, mm**

Legend:
- 350-600d12
- 350-600d10.8
- 350-600d9,7

Why the dipole shifts?

Reflected dipole $\quad d_1 - d_2 = \Delta d$
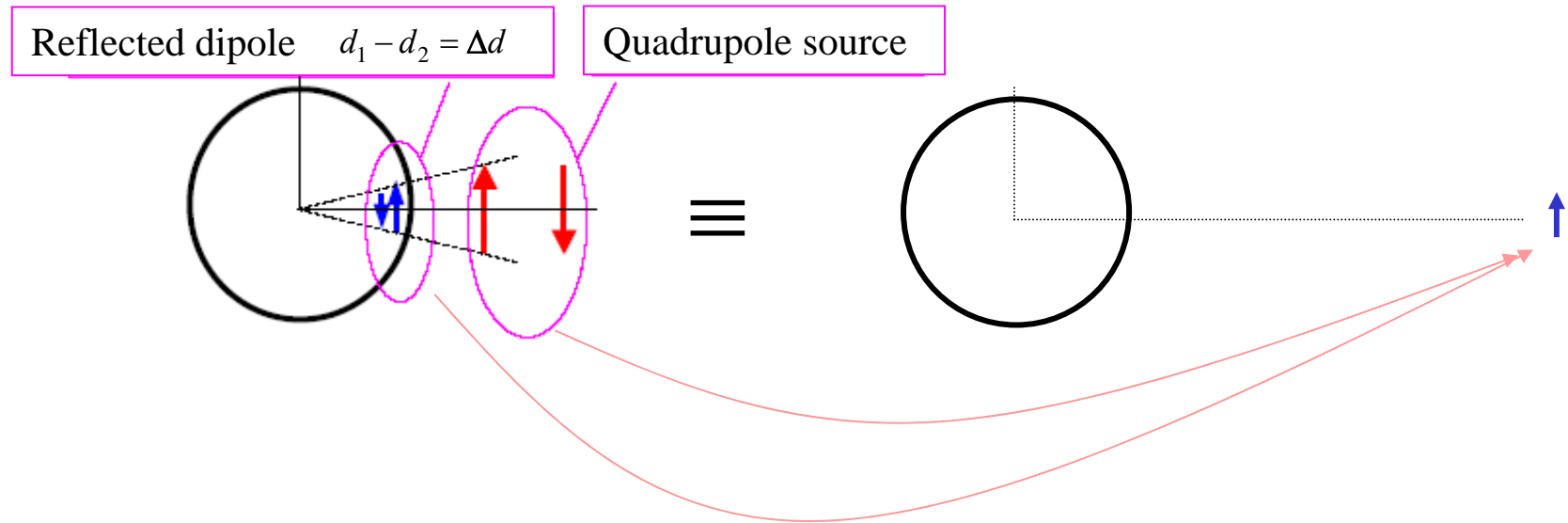
Quadrupole source

$$f(x_0) \approx f(0) + x_0 \cdot f'(0) + \dots$$

dipole + quadrupole = shifted dipole

• It is shown that the effect of the fictitious dipole displacement could be connected with the interference of two sources: (i) quadrupole in the separation zone and (ii) the reflected dipole induced by it.

• Therefore reflected dipole could be generated due to the reflection surface curvature and in far field it exceeds many times the quadrupole in respect with radiation amplitude;

Numerical simulation

Large eddy simulations of the flow past regular cylinders

(TsAGI-ONERA: Eric Manoha and Mark Terracol, 2007)

The three-dimensional filtered unsteady Navier-Stokes equations
written for a viscous compressible fluid

$$\frac{\partial \overline{Q}}{\partial t} + \frac{\partial}{\partial x_i} F_j\left(\overline{Q}\right) - \frac{\partial}{\partial x_i}\left(F_j^v\left(\overline{Q}\right) + F_j^{sgs}\left(\overline{Q}\right)\right) = 0 \qquad \phi = \overline{\phi} + \phi'$$

$\overline{\phi}$ represents the large scale part of the variable, which is directly resolved, and ϕ' its small scale part that will be modelled

$$\overline{Q} = \left(\overline{\rho}, \overline{\rho\tilde{u}_1}, \overline{\rho\tilde{u}_2}, \overline{\rho\tilde{u}_3}, \overline{\rho E}\right)^T$$

F_j the convective fluxes $\qquad F_j^v$ viscous fluxes $\qquad F_j^{sgs}$ subgrid terms

$$F_j\left(\overline{Q}\right) = \begin{pmatrix} \overline{\rho\tilde{u}_j} \\ \overline{\rho\tilde{u}_1\tilde{u}_j} + \delta_{1j}\,\overline{p} \\ \overline{\rho\tilde{u}_2\tilde{u}_j} + \delta_{2j}\,\overline{p} \\ \overline{\rho\tilde{u}_3\tilde{u}_j} + \delta_{3j}\,\overline{p} \\ \left(\overline{\rho E} + \overline{p}\right)\tilde{u}_j \end{pmatrix} \qquad F_j^v\left(\overline{Q}\right) = \begin{pmatrix} 0 \\ \sigma_{1j} \\ \sigma_{2j} \\ \sigma_{3j} \\ \sigma_{kj}\tilde{u}_k + q_j \end{pmatrix} \qquad F_j^{sgs}\left(\overline{Q}\right) = \begin{pmatrix} 0 \\ \tau_{1j} \\ \tau_{2j} \\ \tau_{3j} \\ \tau_{kj}\tilde{u}_k + \varphi_j \end{pmatrix}$$

$$\overline{\rho E} = \frac{\overline{p}}{\gamma - 1} + \frac{1}{2}\overline{\rho\tilde{u}_i\tilde{u}_i} \qquad \varphi_j = \frac{\mu_{sgs}}{\mathrm{Pr}_t}\frac{\partial \tilde{T}}{\partial x_j} \qquad \tau_{ij} = 2\mu_{sgs}\left(S_{ij}\left(\tilde{u}\right) - \frac{1}{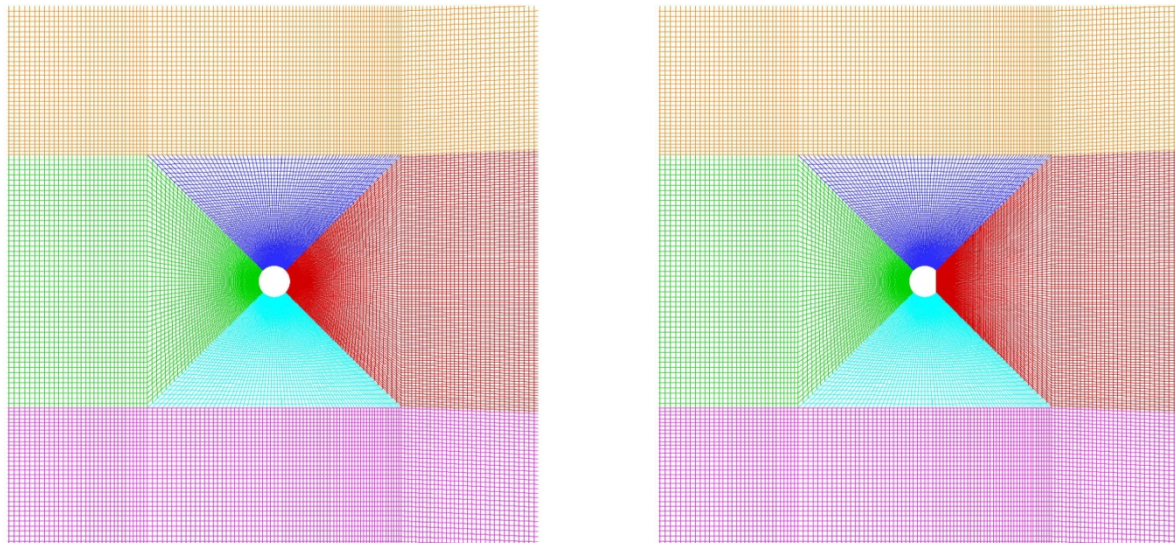3}\delta_{ij}S_{kk}\left(\tilde{u}\right)\right) \qquad S_{ij}\left(\tilde{u}\right) = \frac{1}{2}\left(\frac{\partial \tilde{u}_i}{\partial x_j} + \frac{\partial \tilde{u}_j}{\partial x_i}\right) \qquad q_j\left(\tilde{T}\right) = \frac{\mu\left(\tilde{T}\right)}{\mathrm{Pr}}\frac{\partial \tilde{T}}{\partial x_j}$$

$$\sigma_{ij} = 2\mu\left(\tilde{T}\right)\left(S_{ij}\left(\tilde{u}\right) - \frac{1}{3}\delta_{ij}S_{kk}\left(\tilde{u}\right)\right)$$

Computational setup

The incoming flow has a uniform speed $U_\infty = 70m/s$, and the diameter of the cylinder d is set to $3mm$.

The associated Reynolds number is *Re=15,000*,

3D Configuration
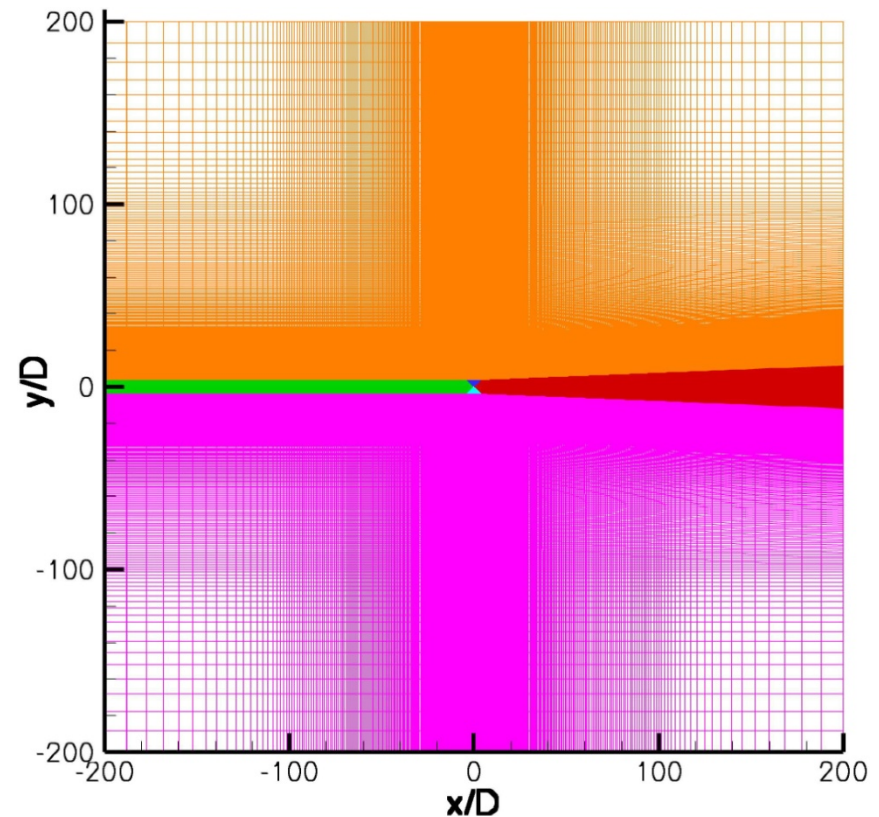
LES (3D) of a realistic Reynolds number configuration

$\rightarrow$ $U_{inf} = 70\ m/s$

$\rightarrow$ $Re_d = 15,000$

$\rightarrow$ $d = 3\ mm$

Same 2D grid section

3D region : spanwise extent = 3d,

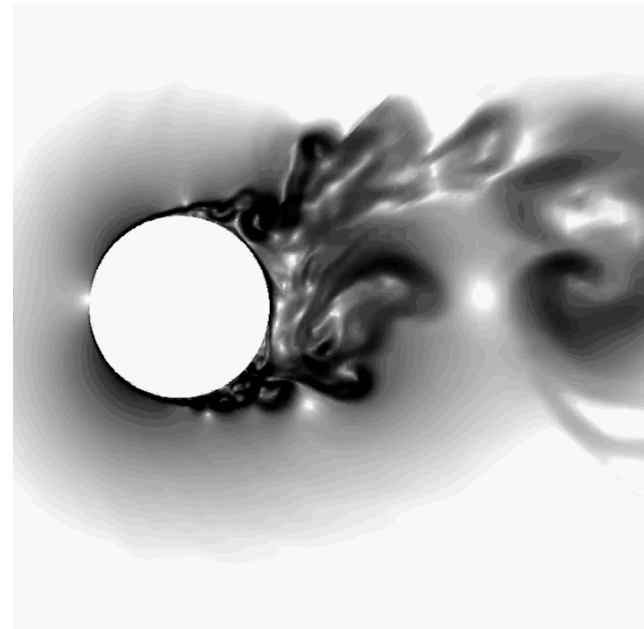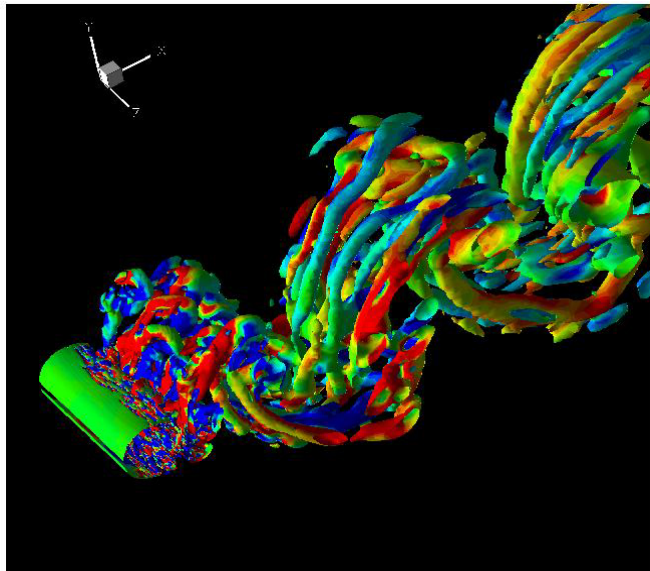30 points

2D/3D grid : 2,000,000 points

Numerical method (*sAbrinA* solver)

- Cell-centered finite volume scheme (2nd order accuracy)

- Spatial derivatives : AUSM + (P) scheme / wiggle detector
(Mary *et al.*, AIAA J., 2002)

- Time : 2nd order implicit scheme ; $CFL_{max} = 12$

- LES : Subgrid model = selective mixed-scale model **(Sagaut *et al.*)**

$$\mu_{sgs} = f_\omega \times \left(\rho C_m \left| \tilde{S} \right|^{1/2} q_{sgs}^{1/4} \Delta^{3/2} \right)$$

Aerodynamic flow features

Baseline

Supercomputers

Lomonosov, MSU

Network	Infiniband
CPUs	Intel EM64T Xeon 55xx 2930 MHz
Number of cores	**35 776**
Nodes	**8 cores** (2 x 4-core CPUs), 12Gb of RAM
Rmax, Tflops	350
Location	Moscow, Russia

MVS-100000, JSC of RAS

Network	Infiniband
CPUs	Intel EM64T Xeon 53xx 3000 MHz
Number of cores	**9472**
Nodes	**8 cores** (2 x 4-core CPUs), 8Gb of RAM
Rmax, Tflops	107
Location	Moscow, Russia

MareNostrum, BSC

Network	Myrinet
CPUs	IBM Power PC 970MP processors at 2.3 GHz
Number of cores	**10240**
Nodes	**4 cores** (2 x 2-core CPUs), 8Gb of RAM
Rmax, Tflops	64
Location	Barcelona, Spain

Supercomputers

Lomonosov, MSU

Network	Infiniband
CPUs	Intel EM64T Xeon 55xx 2930 MHz
Number of cores	**35 776**
Nodes	**8 cores** (2 x 4-core CPUs), 12Gb of RAM
Rmax, Tflops	350
Location	Moscow, Russia

MVS-100000, JSC of RAS

Network	Infiniband
CPUs	Intel EM64T Xeon 53xx 3000 MHz
Number of cores	**9472**
Nodes	**8 cores** (2 x 4-core CPUs), 8Gb of RAM
Rmax, Tflops	107
Location	Moscow, Russia

MareNostrum, BSC

Network	Myrinet
CPUs	IBM Power PC 970MP processors at 2.3 GHz
Number of cores	**10240**
Nodes	**4 cores** (2 x 2-core CPUs), 8Gb of RAM
Rmax, Tflops	64
Location	Barcelona, Spain

A CFD algorithm for compressible flows

The system to solve

$$\frac{\partial \mathbf{Q}}{\partial t} + \frac{\partial \mathbf{F}(\mathbf{Q})}{\partial x} + \frac{\partial \mathbf{G}(\mathbf{Q})}{\partial y} + \frac{\partial \mathbf{H}(\mathbf{Q})}{\partial z} = \frac{1}{Re}\left(\frac{\partial \mathbf{F}_\nu(\mathbf{Q})}{\partial x} + \frac{\partial \mathbf{G}_\nu(\mathbf{Q})}{\partial y} + \frac{\partial \mathbf{H}_\nu(\mathbf{Q})}{\partial z}\right),$$

where **Q** - is a vector of full or linearized conservative variables, **F, G, H** - vectors of full or linearized conservative fluxes, $\mathbf{F}_v$, $\mathbf{G}_v$, $\mathbf{H}_v$ - vectors of full or linearized dissipative fluxes, *Re* - Reynolds number.

Examples of control volumes

The NOISETTE code for CFD/CAA

- **Euler based family of models**
  EE, NSE, NLDE, LEE, LNSE

- **Unstructured tetrahedral meshes**

- **High order numerical schemes***
  Multi-parameter vertex-centered scheme (up to 6th order):
  finite-volume approach for convective terms,
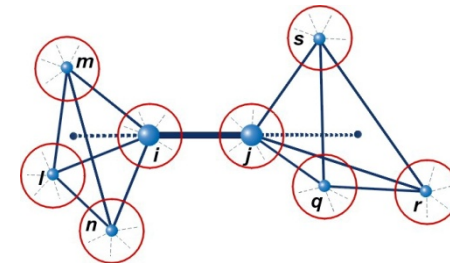 finite-element approach for diffusive terms.

- **Implicit and explicit time integration**
  Explicit Runge-Kutta up to 4-th order
  Implicit up to 2-nd order
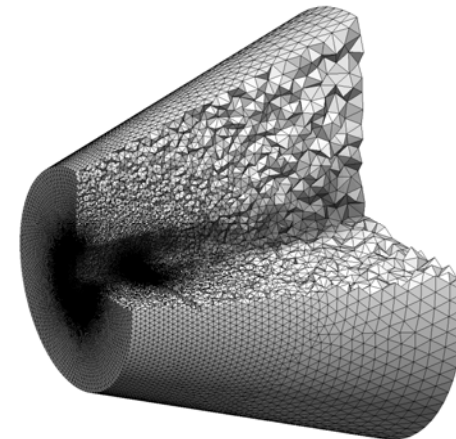
Extended high-order space stencil

* Tatiana Kozubskaya Ilya Abalakin, Alain Dervieux, "High Accuracy Finite Volume
   Method for Solving Nonlinear Aeroacoustics Problems on Unstructured Meshes",
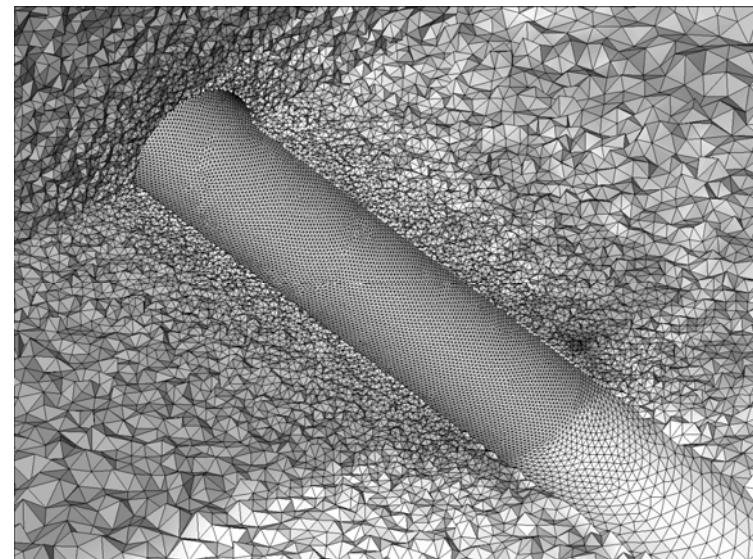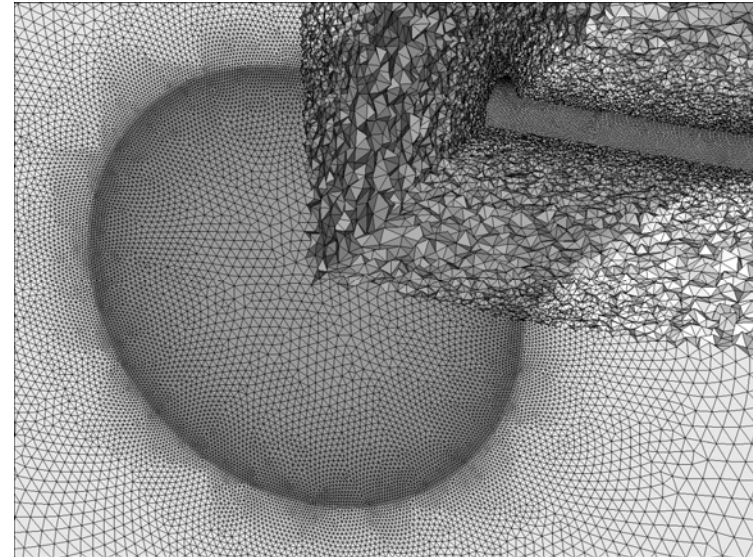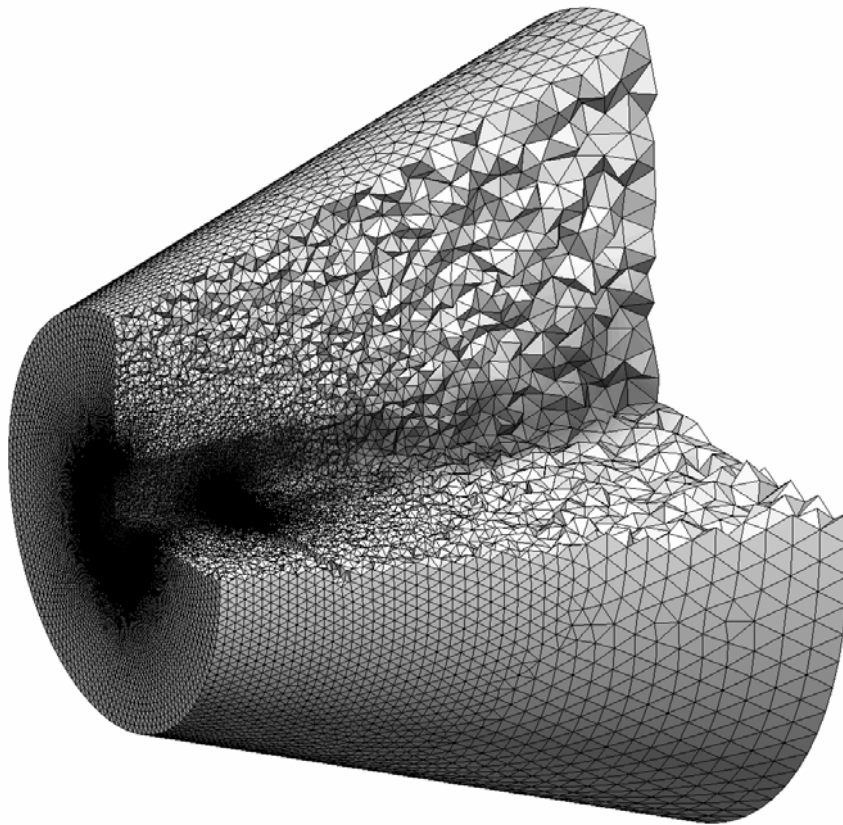   Chinese Journal of Aeroanautics, pages 97-104, 2006.

Example of a tetrahedral mesh

Applications: ILES of compressible flows

Unstructured tetrahedral mesh

- **up to 16M of nodes (~100M tetrahedrons)**

  Mesh in concentrated near the cylinder-jet interaction area and at the jet mixing layer

Applications: ILES of compressible flows

ILES of a round jet interacting with a cylinder: the study of noise sources in the wake
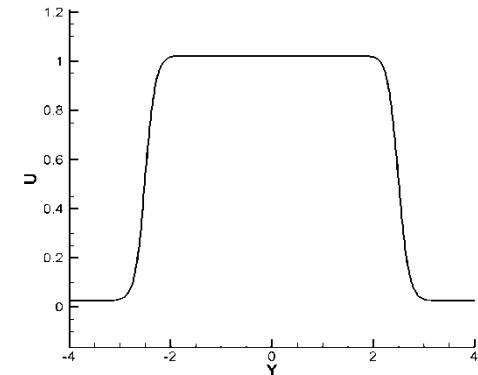
● **Case definition**

• M = 0.206

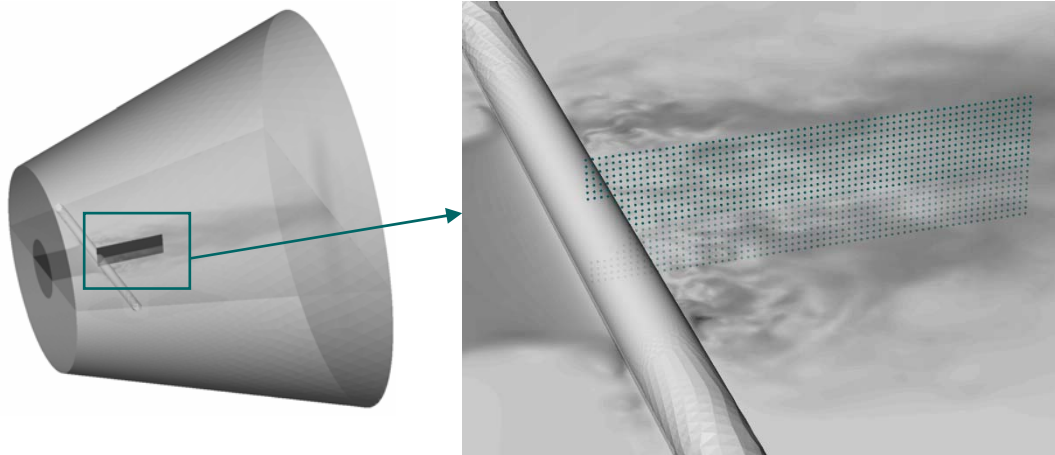• Re = 14000 (based on the diameter of the cylinder)

Experimental part of the study is being performed by **TSAGI**

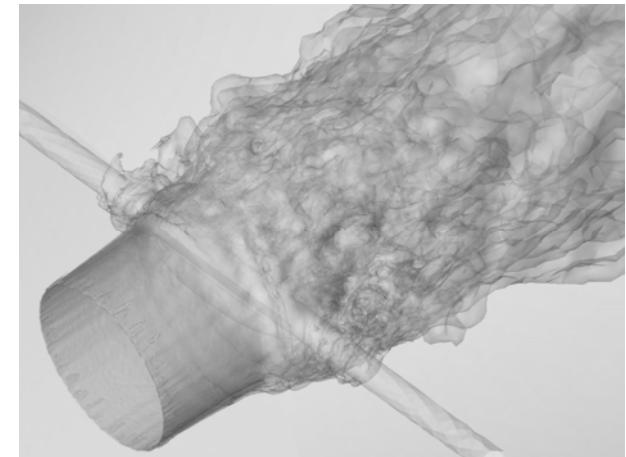Investigations are focused on the aerodynamic noise reduction

1400 control points are placed behind the cylinder

Stationary jet profile with exponential transition

Position of control points

View of the flow
(iso-surfaces of velocity module)
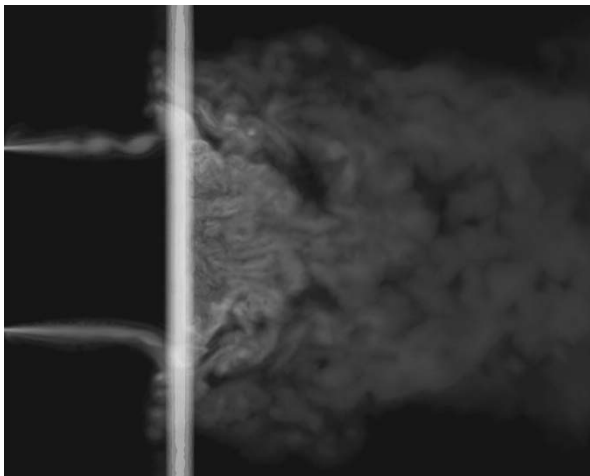
Applications: ILES of compressible flows

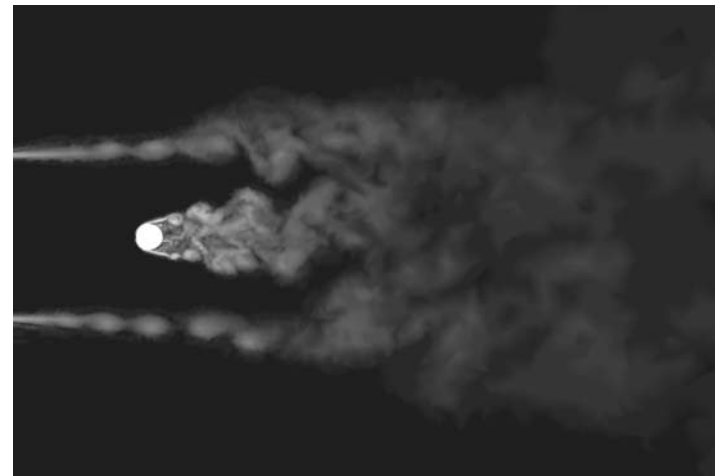**Snapshots at 12% resolution**

Top view   Side view

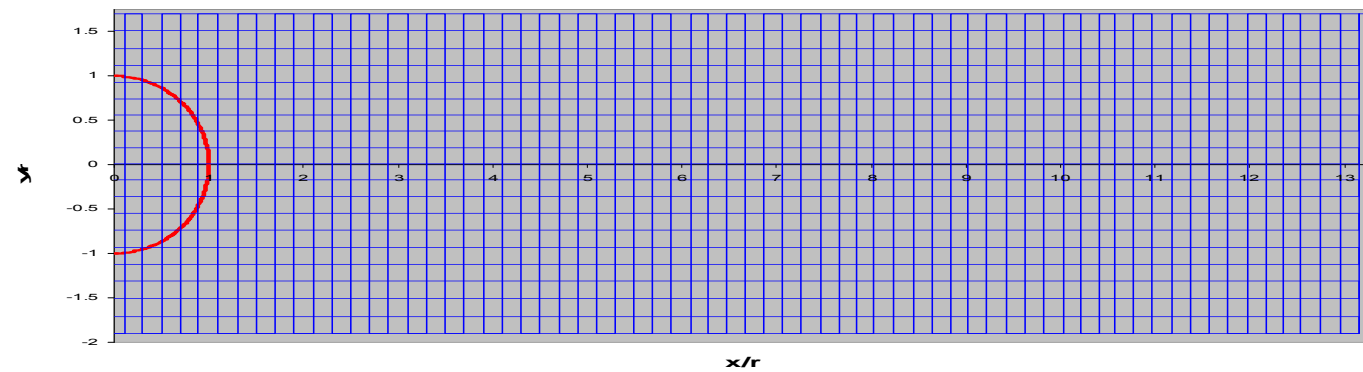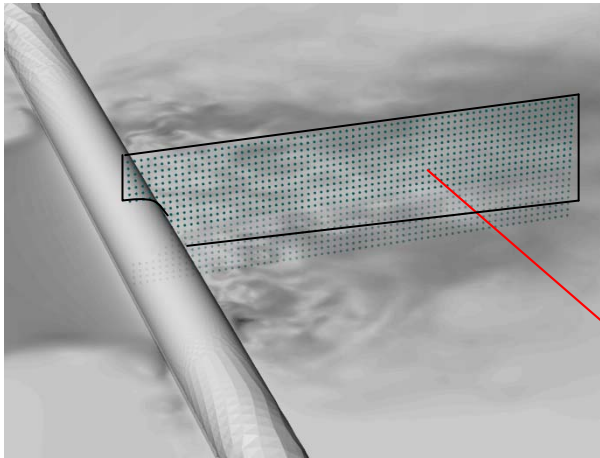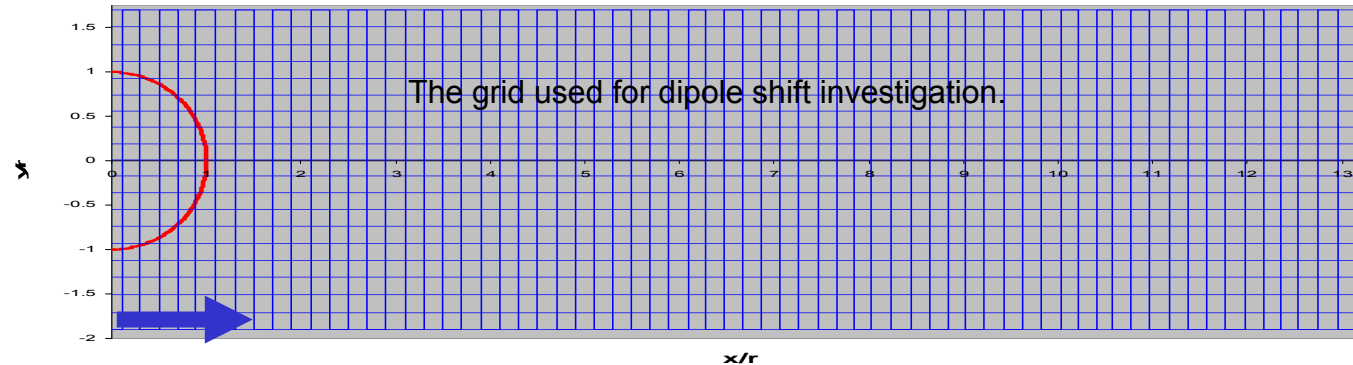Velocity module

Vorticity

Applications: ILES of compressible flows

Visualization of the flow at 12% resolution

2D approach to dipole shift evaluation

2D approach to dipole shift evaluation

The grid used for dipole shift investigation.

$Re = 14000$

The choice of dimensional parameters

$d = 0,003 \text{ m}$

$V_0 = 70 \text{ m/s}$

The quasi two dimensional character of source is the main initial assumption, so data on middle cylinder section corresponding to 2D approach was used from numerical simulation only.

Formulation

$$\left(\frac{1}{c_0^2} \frac{\partial^2}{\partial t^2} - \Delta \right) P = \rho \frac{\partial^2 u_i u_j}{\partial x_i \partial x_j}$$

$$\left. \frac{\partial p}{\partial n} \right|_S = 0 \qquad \text{Boundary condition}$$

multipole decomposition of quadrupole source near the cylinder:
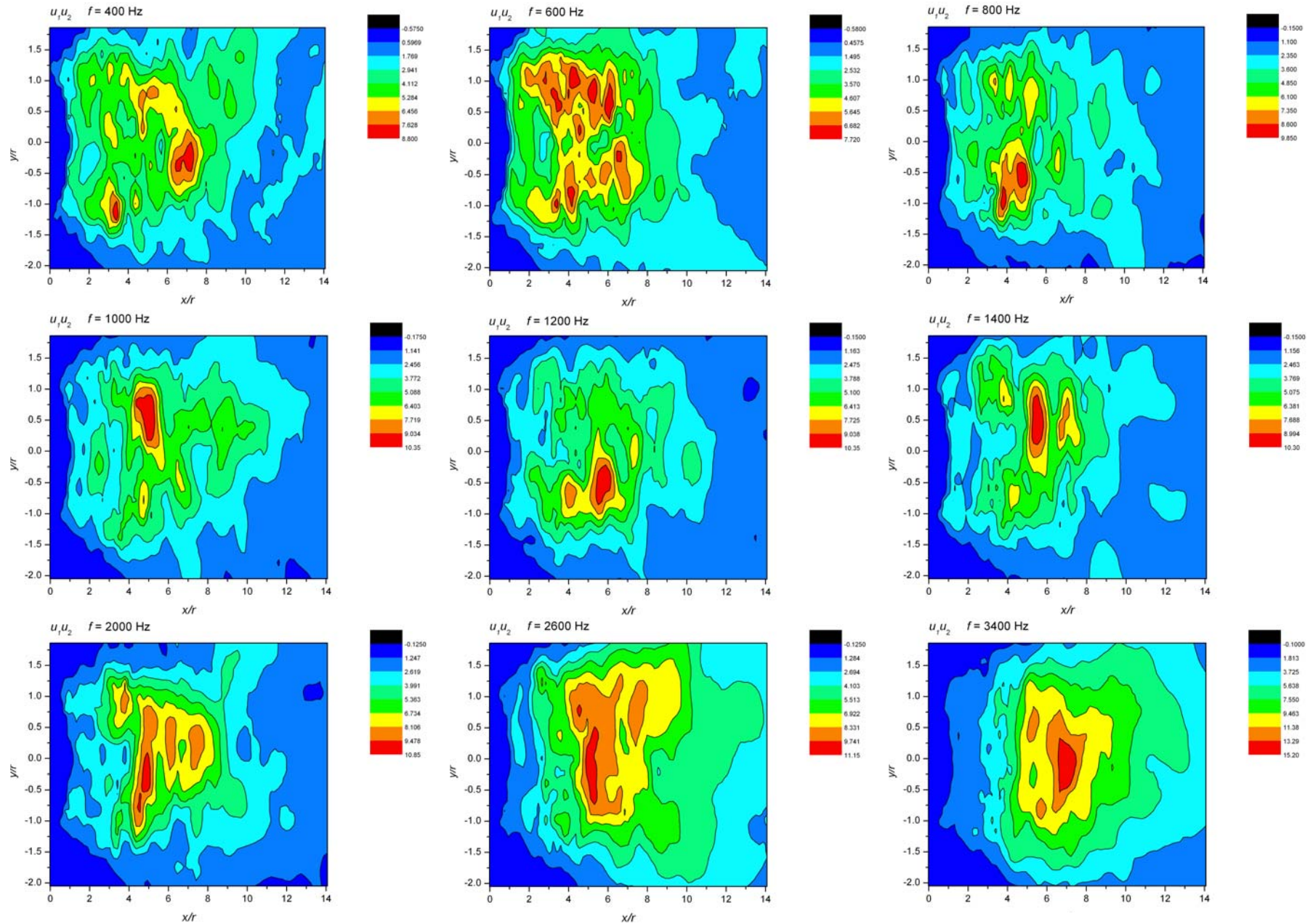it is need to find decomposition origin to cancel quadrupoles moments

$$p = \eta_{(1,0)}\psi_{(1,0)}(\mathbf{x}) + \eta_{(0,1)}\psi_{(0,1)}(\mathbf{x}) + (\mu_{(2,0)} + \eta_{(2,0)} - \mu_{(0,2)} - \eta_{(0,2)})\psi_{(2,0)}(\mathbf{x}) + (\mu_{(1,1)} + \eta_{(1,1)})\psi_{(1,1)}(\mathbf{x}) + \ldots$$

$\psi_\alpha(\mathbf{x}) = (-1)^{|\alpha|} \dfrac{\partial^{|\alpha|} E_0(\mathbf{x})}{\partial x^\alpha}$ - multipoles field; μ_α - multipoles moments of source; η_α - multipoles moments of reflecting field
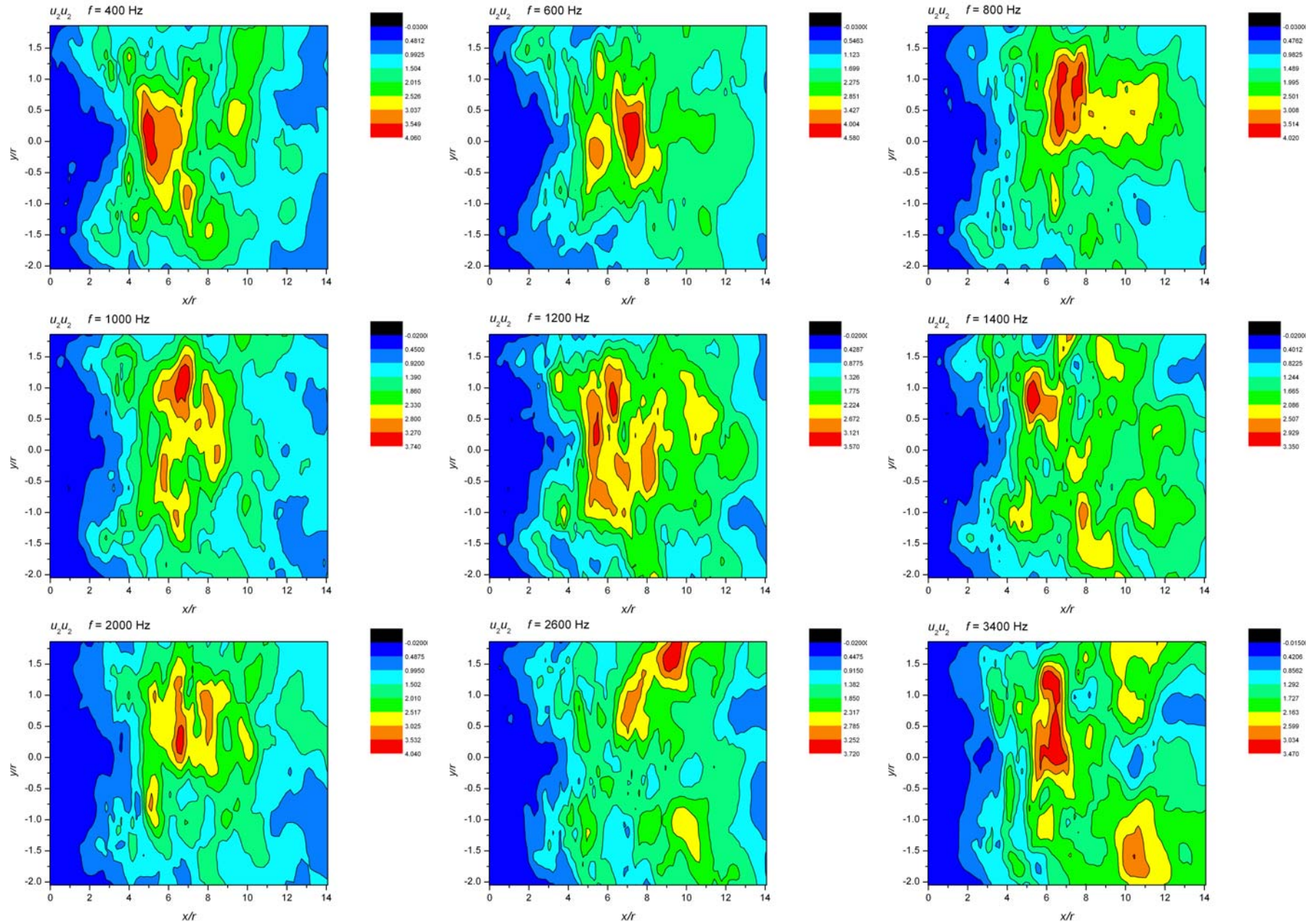
Quadrupole density U1U1 on frequency bands
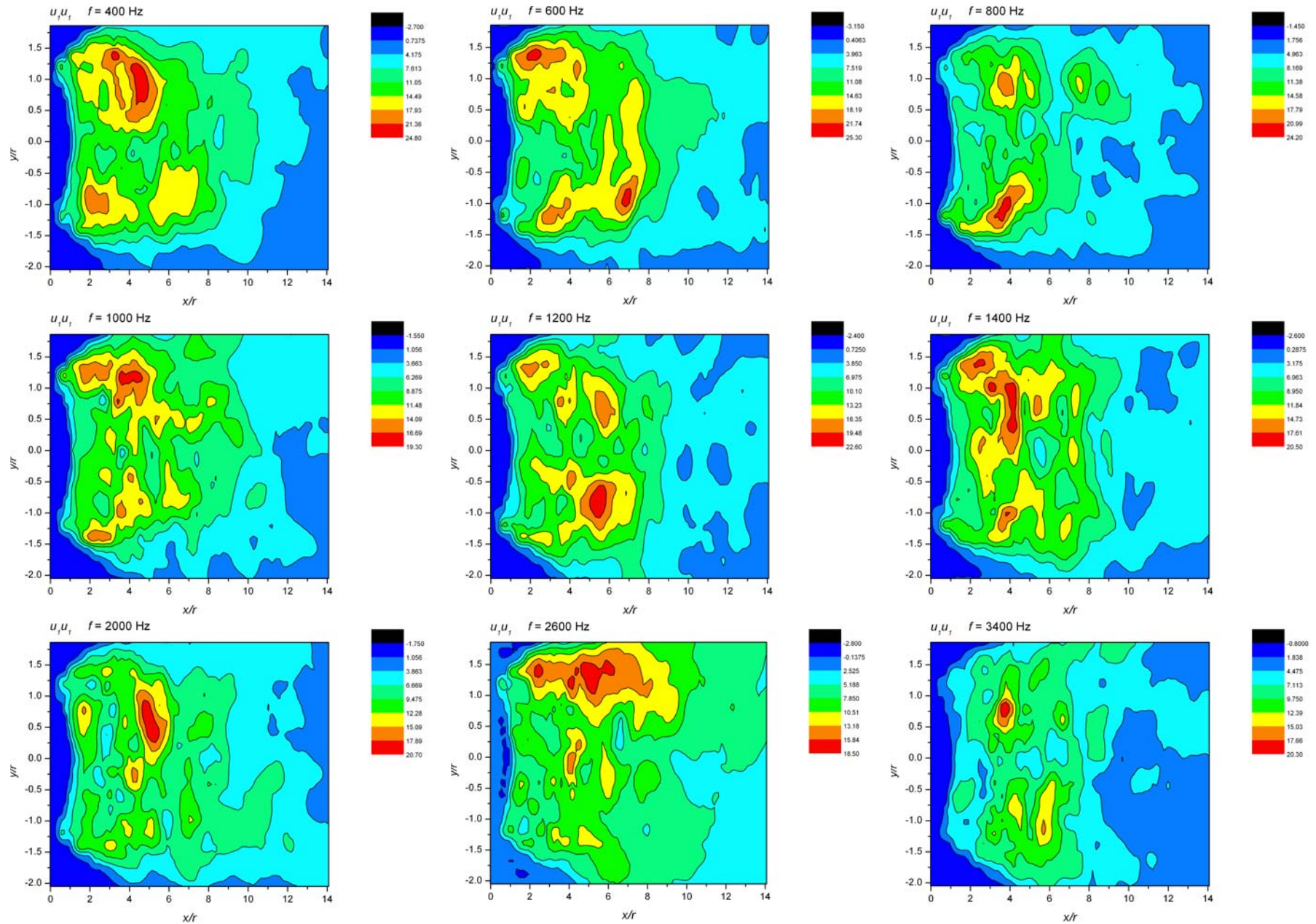
Quadrupole density U1U2 on frequency bands

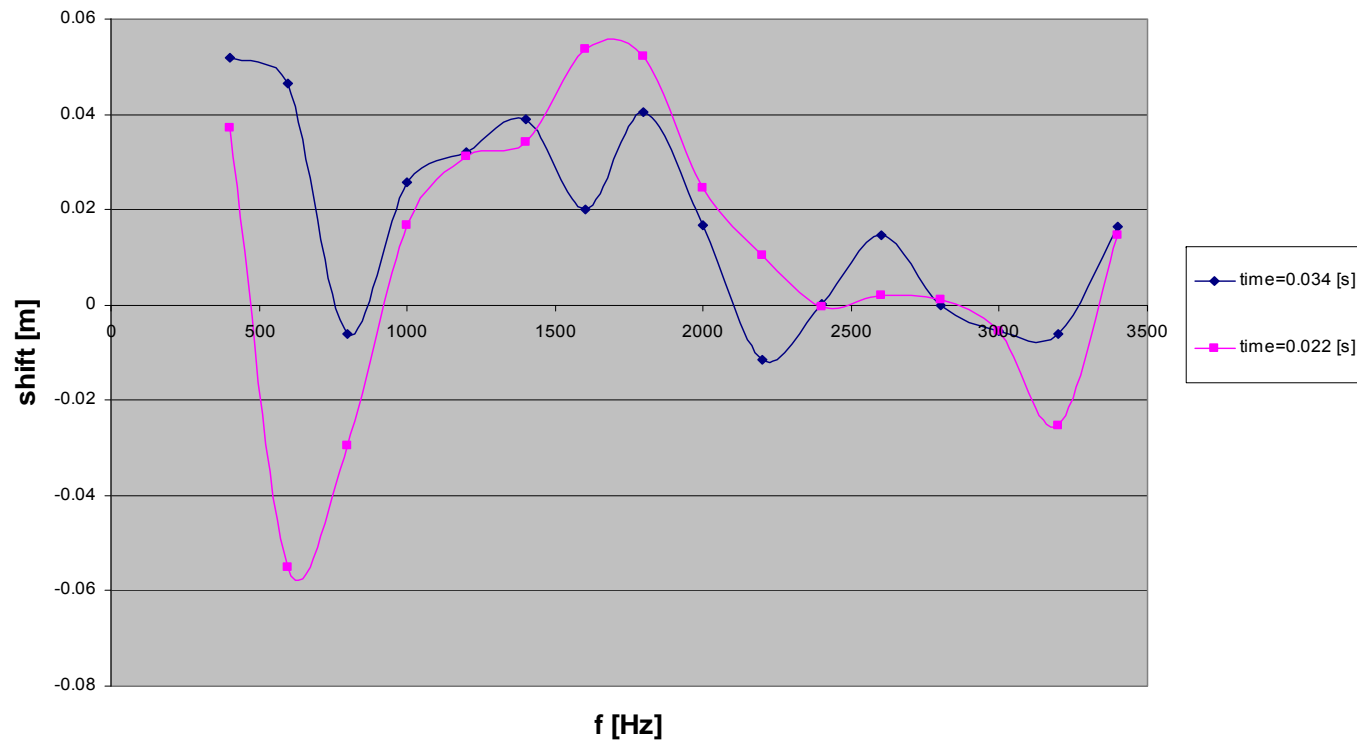# Quadrupole density U2U2 on frequency bands

Frequency dependence of drag dipole shift for Lighthill source

$$\xi_x = \frac{\left\langle \eta_{(1,0)}(\omega)\sigma^*_{(2,0)}(\omega) + \eta^*_{(1,0)}(\omega)\sigma_{(2,0)}(\omega) \right\rangle}{2\left\langle \left| \eta_{(1,0)}(\omega) \right|^2 \right\rangle}$$
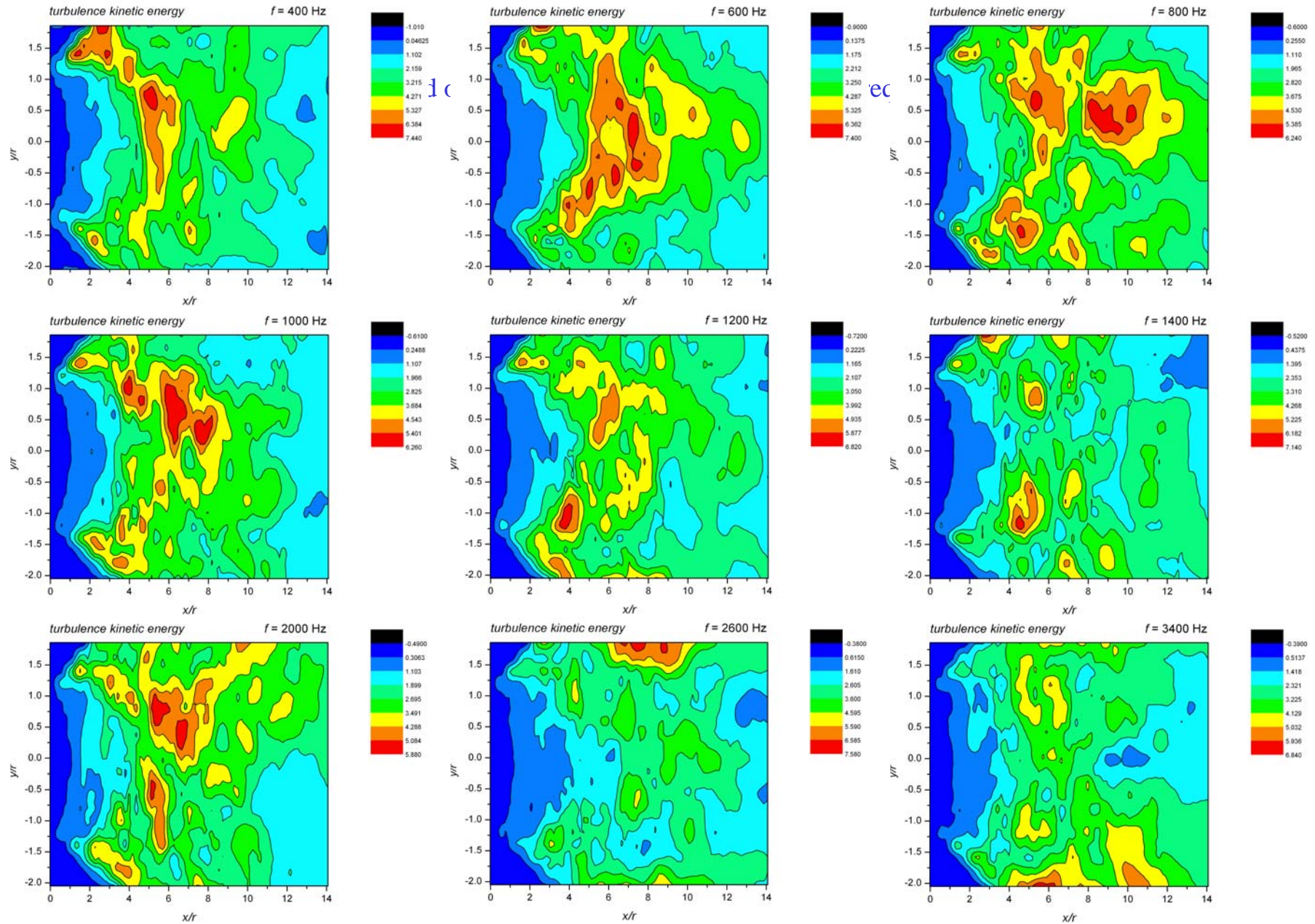
$$\xi_y = 0$$

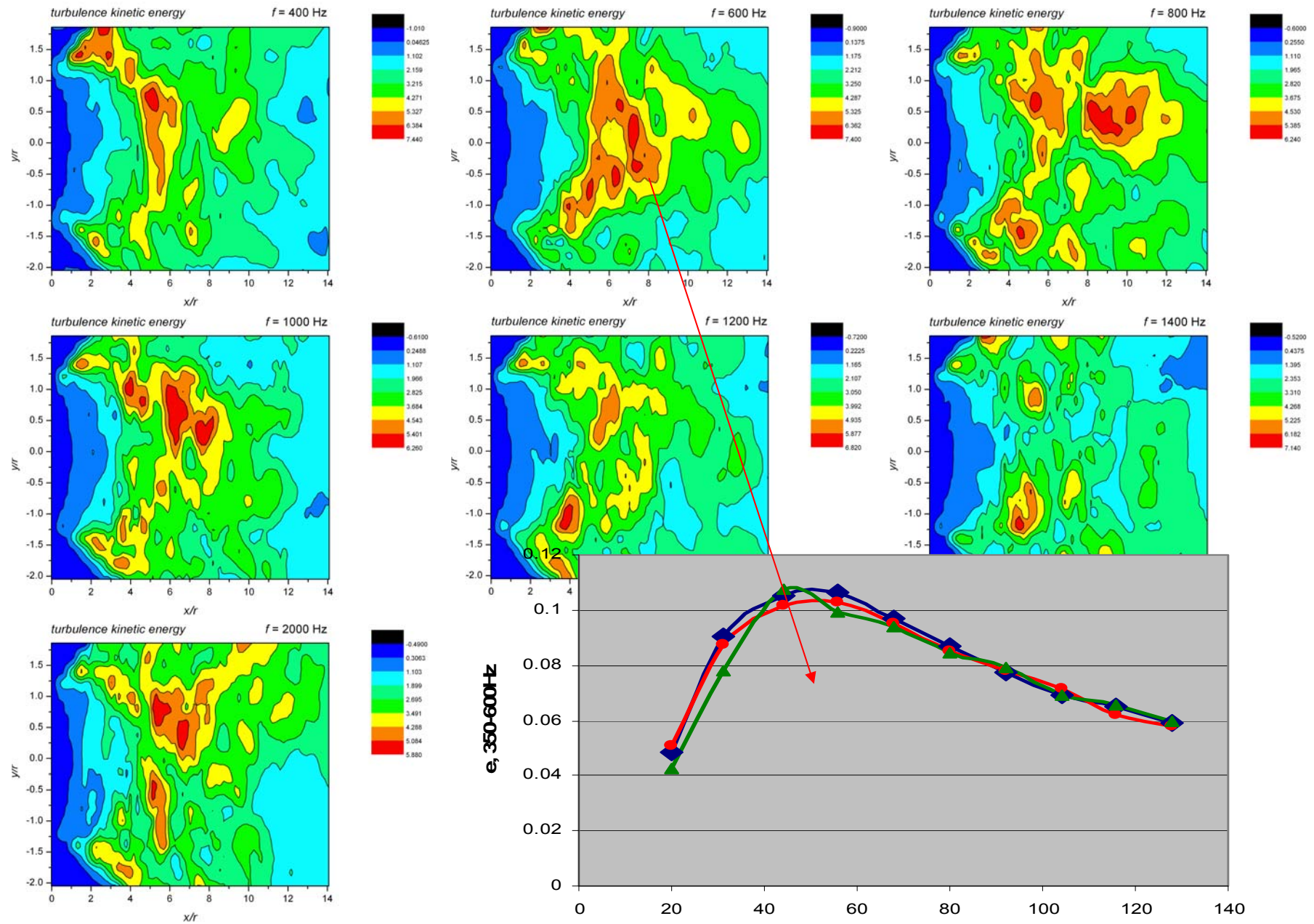dipole shift along x axis is nonlinear characteristic of multipoles moments

There are need a lot of time realization for correct comparing numerical results with experiment

Distribution of mean square velocity pulsation in frequency bands

Distribution of mean square velocity pulsation in frequency bands

Conclusions

- Dipole displacement for rod/jet interaction is demonstrated in experiment using azimuthal decomposition technique;
- It is shown that the effect of the dipole shift is connected with the interference of two sources: quadrupoles in the separation zone and the reflected dipoles induced by them. The reflected dipoles are shown to be generated due to the curvature of reflection surface and their sound pressure level exceeds by many times the quadrupoles in the far field.
- Refraction does not affect main peculiarities of the dipole noise directivity;

- Dipole displacement numerical simulation was considered by TsAGI and IMM teams as a challenging benchmark problem. The most powerful Russian supercomputer (Lomonosov, 350 Tflops) was used;
- ILES for rod/jet interaction was realized using unstructured tetrahedral mesh, Re=14000, (16M of nodes, ~100M tetrahedrons);

- Post processing of numerical data was done. Localization of source density demonstrates the tendency of source accumulation near the axis. However, asymmetry of the source density demonstrates the necessity to improve the simulation;
- Tendency of dipole displacement is recognized as just a tendency. It is necessary to increase the length of the realization to become more sure as to the characteristsics of the source..